Journal of Materials Chemistry A

ROYAL SOCIETY OF CHEMISTRY

PAPER

View Article Online
View Journal

Cite this: DOI: 10.1039/d2ta00019a

Graphene petal foams with hierarchical micro- and nano-channels for ultrafast spontaneous and continuous oil recovery†

Shiwen Wu,[a] Siyu Tian,[a] Ruda Jian,[a] Ting-Nan Wu,[a] Tye David Milazzo,[b] Tengfei Luo*[b] and Guoping Xiong*[a]

Marine oil contamination remediation remains a worldwide challenge. Siphon action provides a spontaneous, continuous, low-cost and green route for oil recovery. However, it is still limited by the low oil recovery rate due to insufficient internal pathways for oil transport. In this paper, a graphene petal foam (GPF)-based oil skimmer is designed and fabricated by plasma-enhanced chemical vapor deposition (PECVD) for ultrafast self-pumping oil recovery from oil/water mixtures. The hierarchical structure, containing micro- and nano-channels formed by interconnected graphene networks and vertically aligned graphene petals (GPs), respectively, and micro-pores inherited from the 3D interconnected structure of Ni foam, provides multiple fast passages for oil transport. An oil recovery rate of 135.2 L m^{-2} h^{-1} is achieved in dark conditions for such oil skimmers, while the value is increased to 318.8 L m^{-2} h^{-1} under solar irradiation of 1 kW m^{-2} because of the excellent solar-heating effect of GPs. Quantitative analyses suggest that 68.8% of such a high oil recovery rate is contributed by the nano-channels and micro-pores, while 31.2% arises from the micro-channels. Our demonstrated GPF oil skimmers exhibit great promise for fast spontaneous and continuous oil contamination cleanup.

Received 1st January 2022
Accepted 6th May 2022

DOI: 10.1039/d2ta00019a

rsc.li/materials-a

Along with the booming development of the oil industry, oil spill and leakage accidents during offshore oil production or marine transportation have resulted in tremendous economic losses and significant damage to the marine environment.[1–3] Since the dissolution of oil in water as well as spreading of oil slicks strongly depends on time, rapid actions are required to separate oil from the bulk water to avoid causing severe damage to the ecosystem once oil spills occur. Physical absorption by porous materials with selective wettability (*e.g.*, oleophilic and hydrophobic surface properties) has become a promising method for oil spill cleanup.[4–6] For example, polydimethylsiloxane-modified graphene nanoribbon aerogels were developed to extract oil from oil/water mixtures.[4] Compared to other conventional methods (*e.g.*, *in situ* combustion[7] and bioremediation[8]), physical absorption provides a green route to clean up oil spills without introducing secondary contaminations. Nevertheless, post-treatments such as pumping or squeezing are generally required to recycle the absorbed oil,[9,10] leading to undesirable complex equipment costs, large energy consumption, and continuous human intervention.

Recently, the siphon effect, relying only on gravitational potential energy difference to continuously transport liquids,[11,12] has been utilized for various applications such as irrigation, oil recovery, and spillway.[13–18] As compared to conventional pump-assisted oil contamination cleanup methods,[19,20] siphon action may provide a spontaneous, continuous, low-cost, and green route with significantly reduced costs. However, low oil transport rate due to many factors such as high viscosity of oil, and physical/chemical properties of channels restricts further development of siphon-assisted oil recovery. To address the issue, light-absorbing materials (*e.g.*, carbon nanotubes,[21] MXene[22]), which directly convert green solar energy to thermal energy (*i.e.*, photothermal effect), have been widely employed to reduce oil viscosity and thus enhance oil transport rate.[21–24] Combining siphon action with photothermal effect provides an effective solution to improve the oil transport rate. In our prior work,[17] a siphon-based oil skimmer equipped with surface-controlled

[a]*Department of Mechanical Engineering, The University of Texas at Dallas, Richardson, Texas 75080, USA. E-mail: guoping.xiong@utdallas.edu*

[b]*Department of Aerospace and Mechanical Engineering, University of Notre Dame, Notre Dame, Indiana 46556, USA. E-mail: tluo@nd.edu*

† Electronic supplementary information (ESI) available: (1) Detailed information on materials, synthesis and characterization of GPF and GPs/Ni; morphology of the compressed Ni foam; morphology of GPs before and after etching the Ni substrate; schematic illustrating the light-trapped capability of GPs; thickness of the GPF oil skimmer; comparison between the GPF oil skimmer and previous oil recovery devices. (2) Accelerated (5000×) video of oil recovery by GPF under 1 sun. (3) Accelerated (5000×) video of oil recovery by GPs/Ni under 1 sun. (4) Accelerated (100×) video of capillary rise of the mineral oil against gravity on GPF skimmer. (5) Accelerated (100×) video of capillary rise of the mineral oil against gravity on GPs/Ni skimmer. See https://doi.org/10.1039/d2ta00019a

nanochannels was designed to achieve self-pumping oil recovery with a recovery rate of 35.2 L m^{-2} h^{-1} in dark condition, and the oil recovery rate was increased to 123.3 L m^{-2} h^{-1} when exposed to solar irradiation of 1 kW m^{-2}. Despite of the enhanced oil recovery rate, the oil recovery process still remains significantly slower compared to conventional techniques relying on electricity-assisted pumping (*e.g.*, over 500 L m^{-2} h^{-1}).[25] Therefore, there is clearly room to further improve the oil recovery rate before the wide-spread adoption of novel siphon oil skimmer strategy for practical applications.

Fluid transport through siphon effect is largely dependent on the properties of the internal channels such as their density and structures.[26,27] Conventional oil recovery materials such as melamine sponge[28,29] and graphene aerogels[30,31] mainly utilize their micro-sized pores for oil transport and usually exhibit relatively low rates because of the insufficient number of internal channels. Therefore, designing multiple transport pathways and rational channel structures are required to achieve efficient siphon-assisted oil recovery. In our prior work, mechanically robust graphene petal foams (GPF) with interconnected hollow internal channels exhibit promising electrochemical performance due to the fast ionic transport properties in the uniquely designed channels.[32] The combination of micro-sized hollow channels and the unique nano-sized structure of graphene petals (GPs) leads to a significantly increased surface area and corresponding outstanding electrical performance. Inspired by the unique structural design, fast oil transport in graphene channels may be achieved by adopting such a unique hierarchical structure with abundant micro- and nano-channels for multiple oil passages.

In this paper, we propose GPF oil skimmers with a uniquely designed hierarchical structure containing micro- and nano-sized all-graphene channels for ultrafast spontaneous and continuous oil recovery. As schematically illustrated in Fig. 1a, free-standing GPF oil skimmers in an inverted U-shape, consisting of vertically aligned GPs on the interconnected three-dimensional (3D) graphene networks, are employed for siphon-assisted self-pumping oil contamination cleanup. The nano-channels are formed by adjacent GPs grown vertically on the Ni substrate through plasma-enhanced chemical vapor deposition (PECVD); and micro-channels are formed by the hollow structure of the 3D graphene network, which is fabricated by chemical etching of the Ni ligaments. Such hierarchical micro- and nano-sized all-graphene channels can provide multiple pathways for efficient oil transport. Moreover, the oleophilic and hydrophobic nature of graphene[33,34] ensures selectively oil transport from oil/water mixtures. Together with the reduced oil viscosity resulting from the outstanding solar-heating effect of GPs,[35–38] stable and efficient oil recovery rates up to 135.2 L m^{-2} h^{-1} and 318.8 L m^{-2} h^{-1} are achieved in dark condition and under 1 sun of illumination (*i.e.*, solar irradiance of 1 kW m^{-2}), respectively, exhibiting great potential in practical applications such as marine oil contamination cleanup without the need of electrical power.

The GPF skimmers are prepared through a two-step process with details described in ESI Materials.† Briefly, GPs are firstly grown on the surface of compressed nickel foams (ESI Fig. S1†) through PECVD. During the PECVD process, GPs with widths ranging from approx. 100–500 nm are densely coated on Ni ligaments and perpendicular to the Ni surface due to the influence of the plasma sheath near the substrate.[39] The adjacent vertically standing GPs on Ni ligaments can form nano-channels for oil transport. Subsequently, Ni ligaments are etched by a facile chemical process,[32] leaving hollow micro-channels in free-standing GPFs. Thus, the GPF skimmers with hierarchical micro- and nano-channels are obtained to further enhance the transport pathways for ultrafast oil recovery. As shown in Fig. 1b, a typical GPF inherits the 3D interconnected structure of Ni ligaments and is highly flexible on a thin Teflon film (inset in Fig. 1b). Oil recovery tests with only Teflon film as an oil skimmer are also conducted for comparison. Results show that no oil is collected after 48 hours (ESI Fig. S2†), indicating that the Teflon substrate exerts no influence on the oil recovery process. The GPF skimmer with an inverted U-shape contains micro-channels with a diameter of several tens of microns (Fig. 1c) and nano-channels with a width ranging from tens of nanometers to hundreds of nanometers (Fig. 1d). Note that the vertically standing GPs in GPFs show negligible structural changes during the etching of Ni foams (ESI Fig. S3†), indicating the good chemical and mechanical stability of GPFs. Moreover, the GPF skimmer exhibits high light absorption performance with an average absorption of 90.0% in dry state and 94.8% when wetted by a mineral oil (Fig. 1e), which can be attributed to the light-trapped capability of the vertically aligned GPs (ESI Fig. S4†).[37,38] As such, solar energy can be efficiently absorbed and transformed to heat by GPFs, which could potentially benefit oil transport by reducing its viscosity.

An ideal skimmer for selective oil transport from oil/water mixtures requires an oleophilic and hydrophobic feature of the channel materials.[17] GPFs are composed of 3D graphene structures which are naturally hydrophobic and oleophilic.[33,34] As shown in Fig. 2a and b, oil droplets can wet the GPF oil skimmer rapidly, while water droplets can stay on the surface of the oil skimmer with a contact angle of 123.6°. The GPF oil skimmers can be treated to be more hydrophobic through thermal reduction, with the water contact angle increased from 123.6° to 138.2° (ESI Fig. S5a†). Nonetheless, the performance of oil recovery barely changes before and after the thermal reduction (ESI Fig. S5b†). Therefore, we believe that the GPF oil skimmers without thermal reduction are sufficient to realize effective oil recovery. We further characterize the capillary rise (h) of the mineral oil against gravity as a function of time in GPF oil skimmers and compare the results with those of control samples (*i.e.*, GPs grown on Ni foams in which Ni ligaments are unetched, denoted as GPs/Ni), as shown in Fig. 2c. ESI Fig. S6† shows the experimental setup, in which two 10 cm-height GPF and GPs/Ni samples are placed vertically, with one end immersed into mineral oil and the other end fixed on a stand. The recorded data of capillary rises as a function of time are fitted by Lucas–Washburn equation, which is widely used to describe capillary rise behavior of liquids.[40,41] The GPF skimmer exhibits excellent oil-transport capability with an oil capillary rise of 5 cm in 12 min because of the capillary forces arising from the micro- and nano-channels. In contrast, it takes 30 min

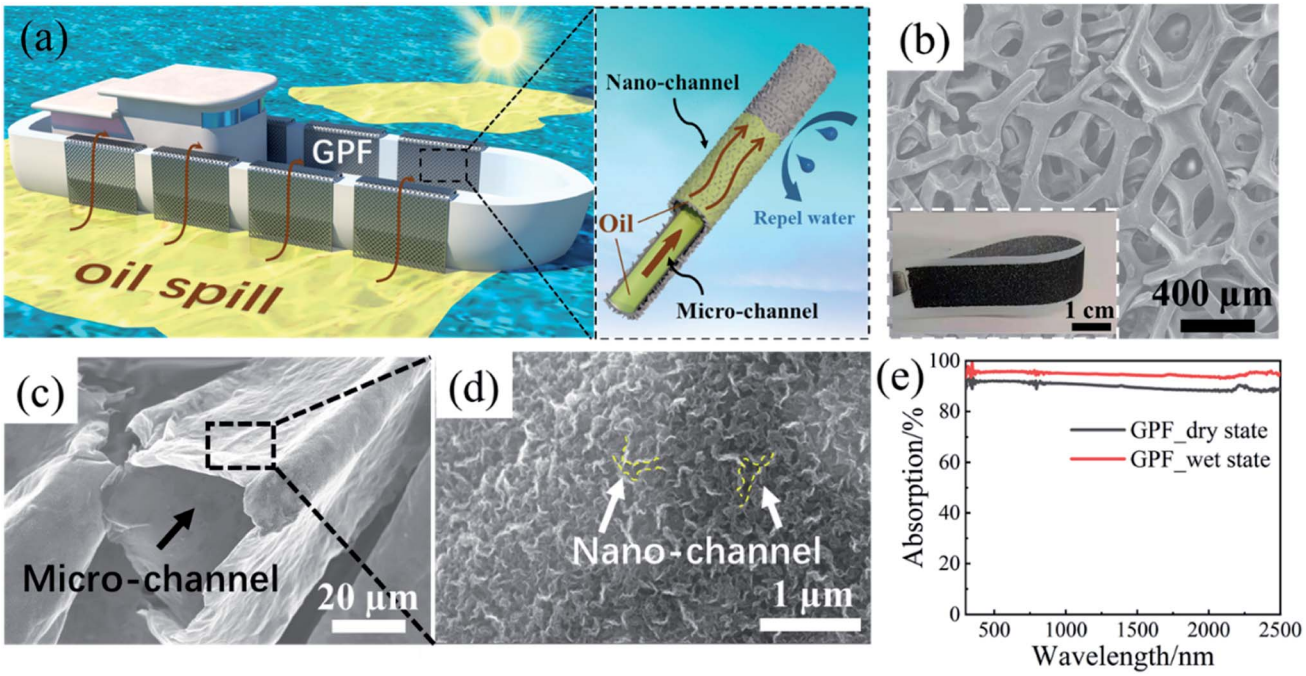

Fig. 1 (a) Schematic illustration of GPFs with hierarchical micro- and nano-channels for efficient solar-enhanced oil recovery. (b) SEM image of the GPF oil skimmer. Insert shows an optical image of the GPF oil skimmer. SEM images of (c) micro-channels and (d) nano-channels in the GPF oil skimmer for oil transports. (e) Absorption curves of the GPF oil skimmer within the solar spectrum under dry and wet states.

for oil to rise 5 cm in the GPs/Ni oil skimmer where only nano-channels contribute to the capillary rise.

Fig. 3a exhibits a schematic of the experimental setup, containing two chambers separated by a wall, for testing oil recovery. A mineral oil/water mixture with a volume ratio of 1 : 1 is added to the left chamber to mimic the floating oil spilled on water, while the right chamber is employed to collect and measure the content of the recovered oil transported from the left one. The two chambers are connected by an inverted U-shape GPF or GPs/Ni oil skimmer, with the height difference between the upper surfaces of oil in the left and right chambers (ΔH, indicated in Fig. 3a) fixed at 40 mm. The oil recovery tests are conducted both in dark condition and under 1 sun of solar illumination. When exposed to the simulated sunlight, both chambers are covered to ensure that only the top surface of oil skimmers are illuminated. As shown in Fig. 3b, the volume of recovered oil by the GPF and GPs/Ni oil skimmers within 24 h are measured by recording the processes using a digital camera (ESI Videos S1 and S2†). Fig. 3d–f present snapshots of oil recovery processes by the GPF skimmers under 1 sun of solar illumination and under dark condition, and by the GPs/Ni oil skimmers under 1 sun of solar illumination. The GPF skimmer

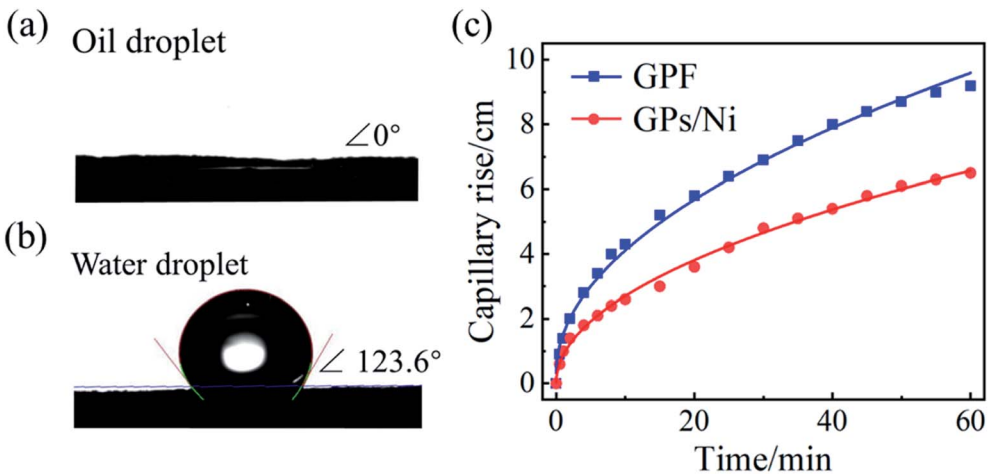

Fig. 2 (a) Oil contact angle and (b) water contact angle measurements of the GPF skimmer. (c) Capillary rises of the mineral oil against gravity as a function of time in GPF and GPs/Ni oil skimmers.

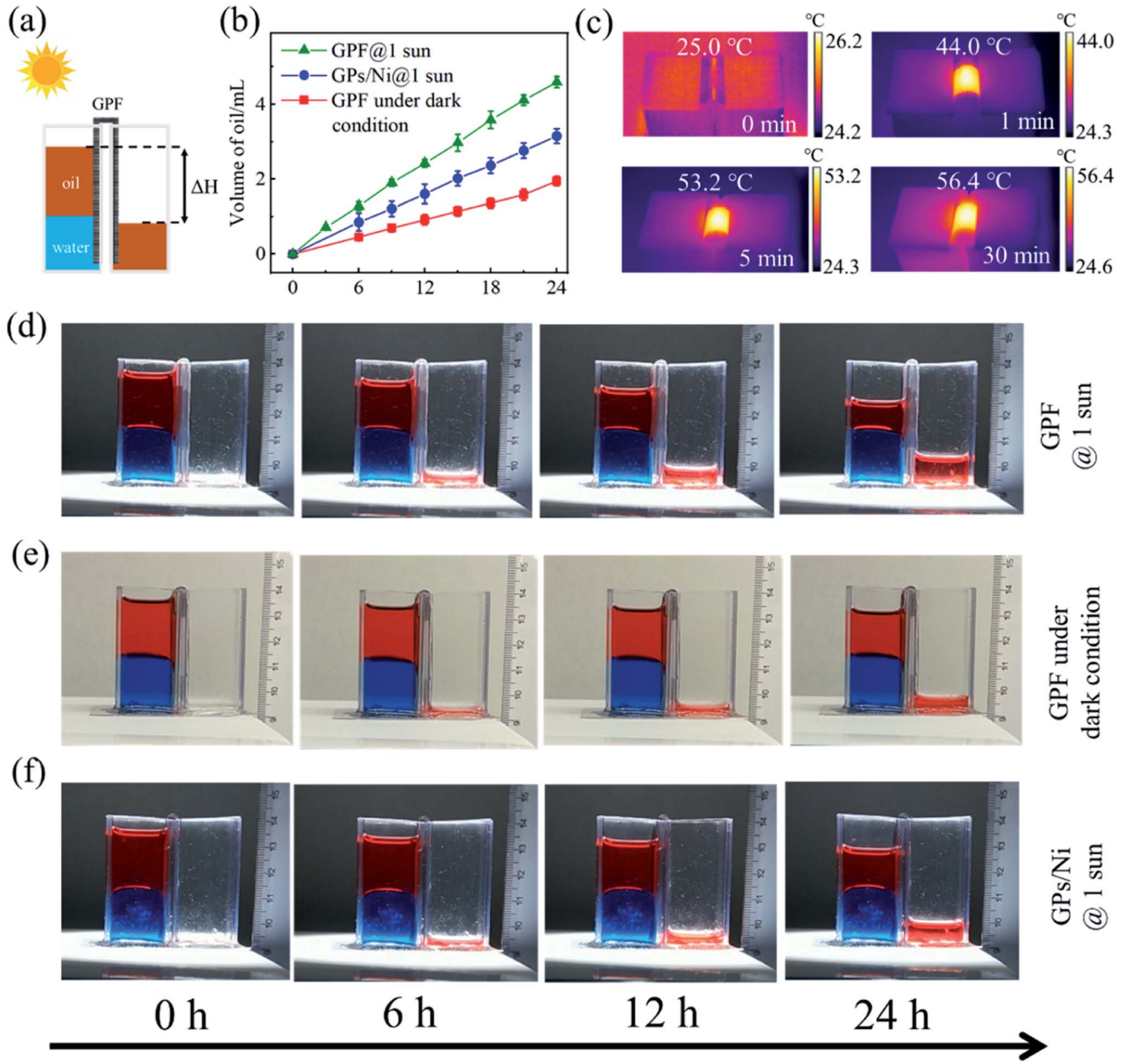

Fig. 3 (a) Schematic illustration of the oil recovery setup. The blue color represents water. The red color represents mineral oil. Oil transports from the oil/water mixture in the left chamber to the right chamber through an inverted U-shape oil skimmer. Δ*H* represents the height difference between the upper surfaces of oil in the left and right chambers. (b) The volume evolutions of recovered oil by GPF and GPs/Ni under different conditions. (c) IR images exhibiting the surface temperature change of GPF working at 1 sun. (d) Optical images showing the oil recovery process by GPF at 1 sun. (e) Optical images showing the oil recovery process by GPF in dark condition. (f) Optical images showing the oil recovery process by GPs/Ni at 1 sun.

exhibits efficient oil transport performance with an average oil recovery rate of 135.2 L m^{-2} h^{-1} in dark condition and 318.8 L m^{-2} h^{-1} under 1 sun of solar illumination. The approximately 2.5-fold enhancement in oil transport rate of the GPF skimmer under solar illumination can be primarily attributed to the decreased oil viscosity under solar irradiation. Fig. 3c shows the surface temperature evolution of the GPF oil skimmer under 1 sun of solar illumination. Due to the outstanding solar absorption properties of GPs, the temperature of the top GPF surface rises quickly from ambient temperature (*i.e.*, 25 °C) to 53.2 °C within 5 min, and then reaches a stable value of approx. 56.2 °C after 30 min. The increasing surface temperature under solar irradiation leads to a decrease in oil viscosity, thereby significantly enhancing the oil recovery rate (Fig. 3b). The GPF oil skimmer exhibits significant improvement of oil transport performance compared to our prior work[17] (*i.e.*, approximately 4-fold and 2.6-fold enhancements in dark condition and under 1 sun of solar illumination, respectively). A comparison of oil recovery rate between our work and other external power-driven oil recovery devices is shown in ESI Table S1.†

The hierarchical structure of the GPF skimmer provides three types of passages for oil transport: nano-channels formed by GPs, micro-channels formed by the etching of Ni ligaments, and micro-pores inherited from the 3D interconnected structure of Ni foam. The contribution of the hollow micro-channels in GPF skimmers can be evaluated by comparing the oil transport rates in GPF and GPs/Ni oil skimmers under 1 sun of solar illumination:

$$\upsilon_m = \frac{\Delta V_{GPF} - \Delta V_{GPs/Ni}}{S\Delta t} \quad (1)$$

where ΔV_{GPF} and $\Delta V_{GPs/Ni}$ represent the volumes of transported oil during a period Δt through the GPF and GPs/Ni oil skimmers under 1 sun, respectively. S represents the cross-sectional area of the GPF oil skimmer which is 10 mm × 0.06 mm (ESI Fig. S7†). From eqn (1), the oil transport rate contributed by micro-channels in the GPF oil skimmers is calculated to be 99.5 L m^{-2} h^{-1} (corresponding to 31.2% of the total oil transport rate). The rest part of the oil transport rate (219.3 L m^{-2} h^{-1}, corresponding to 68.8% of the total oil transport rate) can be attributed to contributions from the nano-channels and micro-pores. In our prior work, we showed that the morphology of GPs could be controlled by changing the growth time during the PECVD process.[42] To investigate the effect of nano-channels on the oil recovery process, GPF skimmers with different nano-channel structures are fabricated by setting the growth time of GPs as 40, 80 and 120 min. SEM images in ESI Fig. S8† show that the GPs are grown more densely as the growth time increases, providing more nano-channels with smaller channel widths for oil transport. The covered areas by GPs are also measured by an open-source software (ImageJ), and the result shows that GPs are covering 16.6%, 24.1%, and 33.0% of the surface of micro-channels as the PECVD growth durations are 40, 80, and 120 min, respectively. According to the Laplace–Young equation, a liquid inside a channel is subjected to capillary force (F_c):[41]

$$F_c = A \times \Delta P_c = A \times 2\sigma \cos\theta / r \quad (2)$$

where A is assumed to be the projected cross-sectional area of the transport channel, ΔP_c is capillary pressure, σ represents the liquid surface tension, θ is the liquid–solid contact angle, and r is the effective pore radius of the transporting channel. The capillary force on the liquid increases as the channel size decreases. Consequently, higher oil recovery rates are achieved in the oil skimmers with a longer growth time of GPs. As shown in Fig. 4a, when the PECVD growth time increases from 40 to 80 and 120 min, the average oil transport rate of the GPF skimmers increases from 239.8 to 281.2 and 318.8 L m^{-2} h^{-1} under 1 sun and increases from 106.4 to 118.8 and 135.2 L m^{-2} h^{-1} in dark condition, respectively. We observe that further decreasing the growth time (*e.g.*, shorter than 40 min) of GPs leads to severe deterioration in the mechanical properties, and structural collapses occur when the GP growth time is excessively short. Therefore, quantitatively determining the contributions from the nano-channels and micro-pores seems rather difficult.

Since siphon action is driven by the change of gravitational potential energy,[12] the height difference between the upper surfaces of oil in the left and right chambers (*i.e.*, ΔH) largely affects the oil recovery rate according to the Bernoulli's relation.[13,17] In this case, the effect of ΔH on the oil recovery performance of GPF oil skimmers under dark condition and 1 sun of illumination is investigated. As shown in Fig. 4b, higher ΔH provides larger gravitational potential energy differences (*i.e.*, larger driving forces) for oil transport, leading to faster oil recovery both under dark condition and at 1 sun. In addition, the intensity of solar irradiation varies in practical applications. Therefore, systematical evaluation of the oil recovery performance of the GPF skimmer under different solar irradiation intensities is highly warranted. Thermal images of the GPF skimmer during oil recovery tests under different solar irradiation intensities are recorded after solar illuminations for 30 min, as shown in Fig. 4c. The surface temperature of the GPF skimmer is promoted notably when the solar irradiation intensity increases. Fig. 4d shows that the viscosity of oil decreases rapidly as the temperature increases. For example, the surface temperature of the GPF skimmer rises from room temperature (*i.e.*, 25 °C) to 56 °C when exposed to 1 sun of solar illumination, leading to a reduction of 69.3% of the oil viscosity and thus a higher oil recovery rate. As shown in Fig. 4e, the GPF oil skimmer exhibits average oil recovery rates of 135.2, 188.9, 244.9, 318.8, and 367.4 L m^{-2} h^{-1} at 0.2, 0.6, 1, and 2 suns of solar illumination, respectively.

In addition, cyclic stability of oil skimmers is another key factor that determines their overall performance in practical applications. We conduct a 10-cycle test (corresponding to 240 h in total) on the oil recovery rate of the GPF oil skimmer under 1 sun, as shown in Fig. 4f. The oil recovery performance exhibits no noticeable degradation during the 240 h test, with the recovery rate remains relatively stable between 300 and 330 L m^{-2} h^{-1}, indicating the excellent long-term cyclic stability of the GPF oil skimmer. Oil recovery tests based on another type of oil (denoted as type 2 oil) with much higher viscosities are conducted on the GPF skimmer (ESI Fig. S9†). Results show that the type 2 oil can also be recovered spontaneously and continuously by the oil skimmer. An average oil recovery rate of 72.8 L m^{-2} h^{-1} is achieved in dark condition, which can be further promoted to 168.0 L m^{-2} h^{-1} under 1 sun of solar illumination, indicating that the photothermal effect is also beneficial for improving the oil transport performance of type 2 oil. Therefore, our proposed GPF oil skimmers are capable to recover oil with a wide viscosity range.

In summary, ultrafast spontaneous and continuous oil recovery from oil/water mixtures is achieved by the unique design of inverted U-shape GPF oil skimmers containing hierarchical micro- and nano-channels. Because of the oleophilic and hydrophobic nature of graphene, GPF oil skimmers show selective oil transport from oil/water mixtures. A typical GPF oil skimmer exhibits a high oil recovery rate of 318.8 L m^{-2} h^{-1} under solar irradiation of 1 kW m^{-2}, which is a 2.5-fold enhancement as compared to that (135.2 L m^{-2} h^{-1}) in dark conditions because of the solar-heating effect of GPs. The contributions from the hierarchical micro- and nano-channels

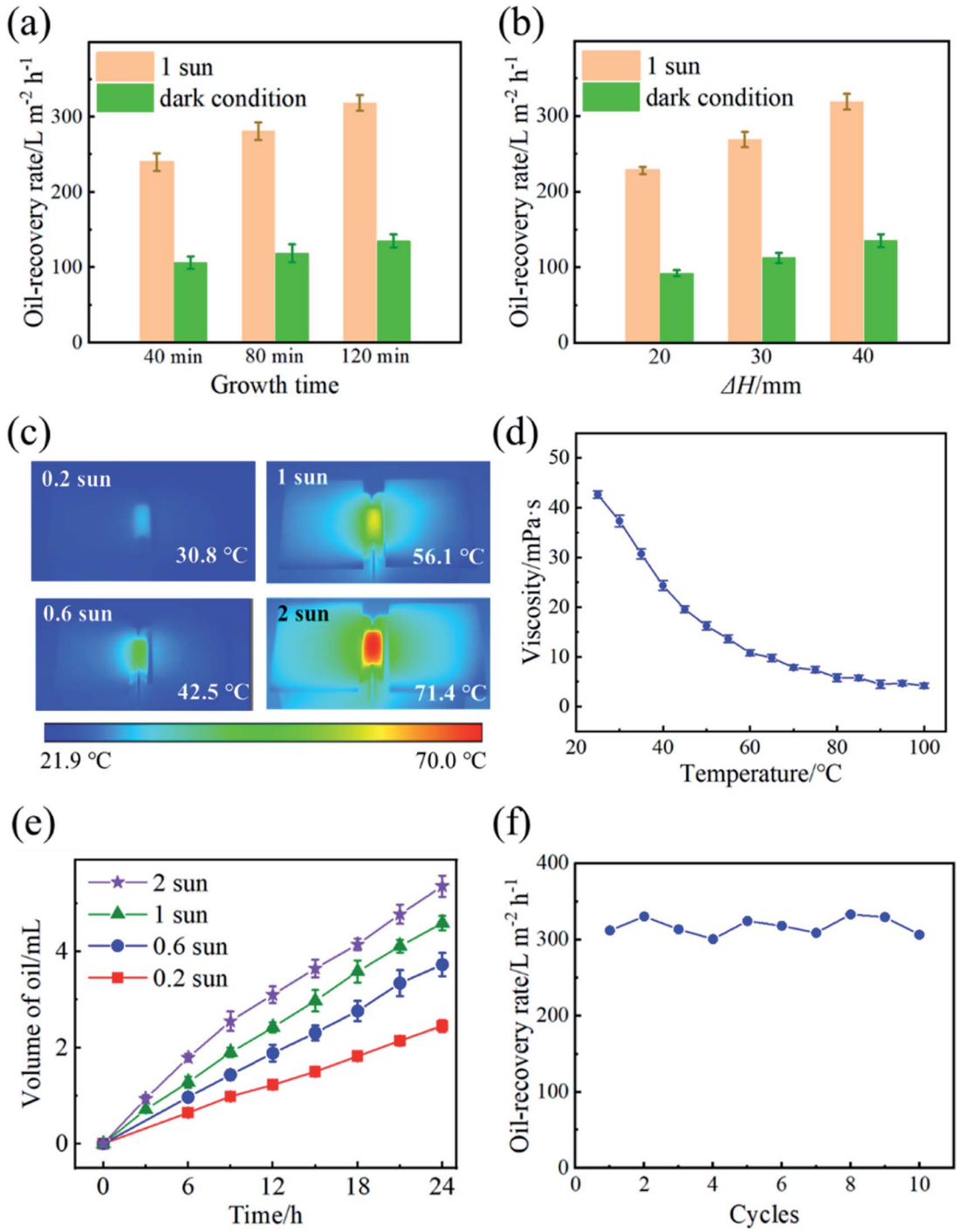

Fig. 4 (a) Average oil transport rates of the GPF oil skimmers with different growth durations of GPs. (b) Comparison of the average oil transport rates of the GPF oil skimmer under different ΔH. (c) IR images exhibiting the surface temperatures of GPF oil skimmer working at 0.2, 0.6, 1, and 2 suns of illumination for 30 min. (d) Viscosities of the mineral oil as a function of temperature. (e) Volume evolutions of recovered oil by GPF skimmers under different solar irradiation intensities. (f) Cyclic stability of the GPF skimmer. Tests are conducted under 1 sun with $\Delta H = 40$ mm.

in the GPF skimmer are quantitatively analyzed by comparing the oil recovery performance of the GPF with GPs/Ni oil skimmers. The results show that 68.8% of the oil recovery rate is contributed by the nano-channels and the micro-pores inherited from the 3D interconnected structure of Ni foam, while 31.2% is contributed by the micro-channels. Moreover, the GPF oil skimmer exhibits long-term cyclic stability during a 240 h oil recovery test. This work provides a novel strategy by combining the hierarchical micro- and nano-channels to achieve fast oil transport without any external power input or assistance of complicated devices, which can also be applied in separation of other liquid mixtures (*e.g.*, water and other organic liquids).

Further optimization of the growth conditions of GPs and geometric parameters of Ni substrates can possibly further enhance the oil recovery rate of GPF oil skimmers that is comparable or even than those of conventional pumping-based oil skimmers.

Conflicts of interest

The authors declare no conflicts of interest.

Acknowledgements

G. X. thanks the University of Texas at Dallas startup fund and the support from the NSF (Grant No. CBET-1937949 and CBET-1949962). T. L. thanks the support from the NSF (Grant No. CBET-1949910 and CBET-1937923). The authors thank Shilin You for the valuable discussion and help during the preparation of the manuscript.

References

1 A. Jernelöv, How to defend against future oil spills, *Nature*, 2010, **466**(7303), 182–183.
2 Q. Ma, H. Cheng, A. G. Fane, R. Wang and H. Zhang, Recent Development of Advanced Materials with Special Wettability for Selective Oil/Water Separation, *Small*, 2016, **12**(16), 2186–2202.
3 **https://www.cnn.com/2021/10/04/us/gallery/california-oil-spill-2021/index.html**.
4 L. Chen, R. Du, J. Zhang and T. Yi, Density controlled oil uptake and beyond: from carbon nanotubes to graphene nanoribbon aerogels, *J. Mater. Chem. A*, 2015, **3**(41), 20547–20553.
5 Z. Xue, Y. Cao, N. Liu, L. Feng and L. Jiang, Special wettable materials for oil/water separation, *J. Mater. Chem. A*, 2014, **2**(8), 2445–2460.
6 M. Peng, Y. Zhu, H. Li, K. He, G. Zeng, A. Chen, Z. Huang, T. Huang, L. Yuan and G. Chen, Synthesis and application of modified commercial sponges for oil-water separation, *Chem. Eng. J.*, 2019, **373**, 213–226.
7 J. Ge, H.-Y. Zhao, H.-W. Zhu, J. Huang, L.-A. Shi and S.-H. Yu, Advanced Sorbents for Oil-Spill Cleanup: Recent Advances and Future Perspectives, *Adv. Mater.*, 2016, **28**(47), 10459–10490.
8 A. J. Pete, B. Bharti and M. G. Benton, Nano-enhanced Bioremediation for Oil Spills: A Review, *ACS ES&T Engg*, 2021, **1**(6), 928–946.
9 H. Niu, J. Li, X. Wang, F. Luo, Z. Qiang and J. Ren, Solar-Assisted, Fast, and In Situ Recovery of Crude Oil Spill by a Superhydrophobic and Photothermal Sponge, *ACS Appl. Mater. Interfaces*, 2021, **13**(18), 21175–21185.
10 R. Zhang, Y. Wu, H. Zhang, S. Xue, M. Guo and T. Zhang, A facile strategy toward hydrophobic–oleophilic 3D Fe foam for efficient oil–water separation, *J. Mater. Sci.*, 2019, **54**(20), 13358–13367.
11 A. Boatwright, S. Hughes and J. Barry, The height limit of a siphon, *Sci. Rep.*, 2015, **5**(1), 16790.
12 J. W. Hicks and H. S. Badeer, Siphon mechanism in collapsible tubes: application to circulation of the giraffe head, *Am. J. Physiol.: Regul., Integr. Comp. Physiol.*, 1989, **256**(2), R567–R571.
13 G. S. Jeong, J. Oh, S. B. Kim, M. R. Dokmeci, H. Bae, S.-H. Lee and A. Khademhosseini, Siphon-driven microfluidic passive pump with a yarn flow resistance controller, *Lab Chip*, 2014, **14**(21), 4213–4219.
14 J. Jin, X. Zhao, Y.-H. Du, M. Ding, C. Xiang, N. Yan, C. Jia, Z. Han and L. Sun, Nanostructured Three-Dimensional Percolative Channels for Separation of Oil-in-Water Emulsions, *iScience*, 2018, **6**, 289–298.
15 H.-y. Sun, D.-f. Wang, Y.-q. Shang, Y.-l. Cai and Z.-l. Wei, An improved siphon drainage method for slope stabilization, *J. Mt. Sci.*, 2019, **16**(3), 701–713.
16 R. Tadayon and A. S. Ramamurthy, Discharge Coefficient for Siphon Spillways, *J. Irrig. Drain. Eng.*, 2013, **139**(3), 267–270.
17 S. Wu, H. Yang, G. Xiong, Y. Tian, B. Gong, T. Luo, T. S. Fisher, J. Yan, K. Cen, Z. Bo and K. K. Ostrikov, Spill-SOS: Self-Pumping Siphon-Capillary Oil Recovery, *ACS Nano*, 2019, **13**(11), 13027–13036.
18 Z. Zhang, Y. Zhang, H. Fan, Y. Wang, C. Zhou, F. Ren, S. Wu, G. Li, Y. Hu, J. Li, D. Wu and J. Chu, A Janus oil barrel with tapered microhole arrays for spontaneous high-flux spilled oil absorption and storage, *Nanoscale*, 2017, **9**(41), 15796–15803.
19 J. Ge, L.-A. Shi, Y.-C. Wang, H.-Y. Zhao, H.-B. Yao, Y.-B. Zhu, Y. Zhang, H.-W. Zhu, H.-A. Wu and S.-H. Yu, Joule-heated graphene-wrapped sponge enables fast clean-up of viscous crude-oil spill, *Nat. Nanotechnol.*, 2017, **12**(5), 434–440.
20 Y. Huang, T. Gancheva, B. D. Favis, A. Abidli, J. Wang and C. B. Park, Hydrophobic Porous Polypropylene with Hierarchical Structures for Ultrafast and Highly Selective Oil/Water Separation, *ACS Appl. Mater. Interfaces*, 2021, **13**(14), 16859–16868.
21 X. Wu, Y. Lei, S. Li, J. Huang, L. Teng, Z. Chen and Y. Lai, Photothermal and Joule heating-assisted thermal management sponge for efficient cleanup of highly viscous crude oil, *J. Hazard. Mater.*, 2021, **403**, 124090.
22 X. Ma, K. Chen, S. Li, P. Gnanasekar, Y. Zhong, Y. An, Q. Luo, Q. Huang, J. Zhu, J. Chen and N. Yan, Degradable Ti3C2Tx MXene Nanosheets Containing a Lignin Polyurethane Photothermal Foam (LPUF) for Rapid Crude Oil Cleanup, *ACS Appl. Nano Mater.*, 2022, **5**(2), 2848–2858.
23 W. Chao, S. Wang, Y. Li, G. Cao, Y. Zhao, X. Sun, C. Wang and S.-H. Ho, Natural sponge-like wood-derived aerogel for solar-assisted adsorption and recovery of high-viscous crude oil, *Chem. Eng. J.*, 2020, **400**, 125865.
24 Q. Li, Q. Sun, Y. Li, T. Wu, S. Li, H. Zhang and F. Huang, Solar-Heating Crassula perforata-Structured Superoleophilic CuO@CuS/PDMS Nanowire Arrays on Copper Foam for Fast Remediation of Viscous Crude Oil Spill, *ACS Appl. Mater. Interfaces*, 2020, **12**(17), 19476–19482.
25 S. He, X. Cheng, Z. Li, X. Shi, H. Yang and H. Zhang, Green and facile synthesis of sponge-reinforced silica aerogel and its pumping application for oil absorption, *J. Mater. Sci.*, 2016, **51**(3), 1292–1301.

26 V. Narayanamurthy, Z. E. Jeroish, K. S. Bhuvaneshwari, P. Bayat, R. Premkumar, F. Samsuri and M. M. Yusoff, Advances in passively driven microfluidics and lab-on-chip devices: a comprehensive literature review and patent analysis, *RSC Adv.*, 2020, **10**(20), 11652–11680.

27 P. Wang, S. Yuan, N. Yang and P. K. Oppong, A comprehensive review on non-active micro-pumps for microfluidic platforms, *J. Micromech. Microeng.*, 2021, **31**(9), 093001.

28 A. Stolz, S. Le Floch, L. Reinert, S. M. M. Ramos, J. Tuaillon-Combes, Y. Soneda, P. Chaudet, D. Baillis, N. Blanchard, L. Duclaux and A. San-Miguel, Melamine-derived carbon sponges for oil-water separation, *Carbon*, 2016, **107**, 198–208.

29 C.-F. Wang, H.-C. Huang and L.-T. Chen, Protonated Melamine Sponge for Effective Oil/Water Separation, *Sci. Rep.*, 2015, **5**(1), 14294.

30 L. Xu, G. Xiao, C. Chen, R. Li, Y. Mai, G. Sun and D. Yan, Superhydrophobic and superoleophilic graphene aerogel prepared by facile chemical reduction, *J. Mater. Chem. A*, 2015, **3**(14), 7498–7504.

31 S. Yang, C. Shen, L. Chen, C. Wang, M. Rana and P. Lv, Vapor–Liquid Deposition Strategy To Prepare Superhydrophobic and Superoleophilic Graphene Aerogel for Oil–Water Separation, *ACS Appl. Nano Mater.*, 2018, **1**(2), 531–540.

32 G. Xiong, P. He, D. Wang, Q. Zhang, T. Chen and T. S. Fisher, Hierarchical Ni–Co Hydroxide Petals on Mechanically Robust Graphene Petal Foam for High-Energy Asymmetric Supercapacitors, *Adv. Funct. Mater.*, 2016, **26**(30), 5460–5470.

33 S. V. Thakkar, A. Pinna, C. M. Carbonaro, L. Malfatti, P. Guardia, A. Cabot and M. F. Casula, Performance of oil sorbents based on reduced graphene oxide–silica composite aerogels, *J. Environ. Chem. Eng.*, 2020, **8**(1), 103632.

34 S. Wu, B. Gong, H. Yang, Y. Tian, C. Xu, X. Guo, G. Xiong, T. Luo, J. Yan, K. Cen, Z. Bo, K. K. Ostrikov and T. S. Fisher, Plasma-Made Graphene Nanostructures with Molecularly Dispersed F and Na Sites for Solar Desalination of Oil-Contaminated Seawater with Complete In-Water and In-Air Oil Rejection, *ACS Appl. Mater. Interfaces*, 2020, **12**(34), 38512–38521.

35 Y. Tian, H. Yang, S. Wu, J. Yan, K. Cen, T. Luo, G. Xiong, Y. Hou, Z. Bo and K. Ostrikov, Beyond lotus: Plasma nanostructuring enables efficient energy and water conversion and use, *Nano Energy*, 2019, **66**, 104125.

36 S. Wu, G. Xiong, H. Yang, B. Gong, Y. Tian, C. Xu, Y. Wang, T. Fisher, J. Yan, K. Cen, T. Luo, X. Tu, Z. Bo and K. Ostrikov, Multifunctional Solar Waterways: Plasma-Enabled Self-Cleaning Nanoarchitectures for Energy-Efficient Desalination, *Adv. Energy Mater.*, 2019, **9**(30), 1901286.

37 S. Wu, G. Xiong, H. Yang, Y. Tian, B. Gong, H. Wan, Y. Wang, T. S. Fisher, J. Yan, K. Cen, Z. Bo and K. Ostrikov, Scalable Production of Integrated Graphene Nanoarchitectures for Ultrafast Solar-Thermal Conversion and Vapor Generation, *Matter*, 2019, **1**(4), 1017–1032.

38 C. Xu, Z. Bo, S. Wu, Z. Wen, J. Chen, T. Luo, E. Lee, G. Xiong, R. Amal, A. T. S. Wee, J. Yan, K. Cen, T. S. Fisher and K. Ostrikov, Vertical graphene nano-antennas for solar-to-hydrogen energy conversion, *Sol. Energy*, 2020, **208**, 379–387.

39 S. Tian, S. Wu and G. Xiong, Graphitic nanopetals and their applications in electrochemical energy storage and biosensing, *J. Nanopart. Res.*, 2020, **22**(5), 97.

40 Y. Tsunazawa, T. Yokoyama and N. Nishiyama, An experimental study on the rate and mechanism of capillary rise in sandstone, *Prog. Earth Planet. Sci.*, 2016, **3**(1), 8.

41 J. Cai, E. Perfect, C.-L. Cheng and X. Hu, Generalized Modeling of Spontaneous Imbibition Based on Hagen–Poiseuille Flow in Tortuous Capillaries with Variably Shaped Apertures, *Langmuir*, 2014, **30**(18), 5142–5151.

42 G. Xiong, K. P. S. S. Hembram, D. N. Zakharov, R. G. Reifenberger and T. S. Fisher, Controlled thin graphitic petal growth on oxidized silicon, *Diamond Relat. Mater.*, 2012, **27–28**, 1–9.

